Modelling protein complexes with crosslinking mass spectrometry and deep learning

Kolja Stahl[1], Lorenz Demann[2], Rica Bremenkamp[2], Robert Warneke[2], Björn Hormes[2], Jörg Stülke[2], Oliver Brock[3], Juri Rappsilber[1,4,5,§]

[1] Technische Universität Berlin, Chair of Bioanalytics, 10623 Berlin, Germany
[2] Georg-August-Universität Göttingen, Department of General Microbiology, Institute for Microbiology & Genetics, GZMB, 37077 Göttingen, Germany
[3] Technische Universität Berlin, Robotics and Biology Laboratory, 10623 Berlin, Germany
[4] Si-M/"Der Simulierte Mensch", a Science Framework of Technische Universität Berlin and Charité - Universitätsmedizin Berlin, 10623 Berlin, Germany.
[5] Wellcome Centre for Cell Biology, University of Edinburgh, Edinburgh EH9 3BF, UK

[§] corresponding author: juri.rappsilber@tu-berlin.de

Scarcity of structural and evolutionary information on protein complexes poses a challenge to deep learning-based structure modelling. We integrated experimental distance restraints obtained by crosslinking mass spectrometry (MS) into AlphaFold-Multimer, by extending AlphaLink to protein complexes. Integrating crosslinking MS data substantially improves modelling performance on challenging targets, by helping to identify interfaces, focusing sampling, and improving model selection. This extends to single crosslinks from whole-cell crosslinking MS, opening the possibility of whole-cell structural investigations driven by experimental data. We demonstrate this by revealing the molecular basis of iron homeostasis in *Bacillus subtilis*.

Solving the structure of protein complexes is key to understanding life at the molecular level. The advent of deep learning-based methods has significantly improved the reliability of single protein structure prediction[1]. However, the general lack of co-evolutionary information and the lower number of solved structures makes predicting the structure of protein complexes a more difficult task[2]. Experimental distance restraints, such as proximal residue pairs revealed by crosslinking MS, can identify interactions[3–5] and their interfaces[6]. The experimental information can supplement information derived from evolutionary relationships in guiding structure prediction[7].

In our previous work, we improved modelling of challenging single protein targets by leveraging distance restraints in AlphaLink[7], a deep learning-based method that integrates crosslinking mass spectrometry (MS) data directly into the pair representation of AlphaFold2[1] to bias the prediction. Here, we extend AlphaLink to protein complexes. Protein complexes pose a much harder problem because on top of predicting the structure of the individual chains, predicting

interactions requires searching a space that grows exponentially with the size of the complex. Crosslinking MS data can help to cut down the search space and reduce the dependency of the prediction on evolutionary information.

In this study, we train with succinimidyl 4,4-azipentanoate (SDA) crosslinks but successfully test also with a different crosslinker. SDA is a soluble crosslinker that provides restraints between residues receptive to its first reaction step, Lys, Ser, Thr and Tyr, and other amino acids on protein surfaces[8]and is readily available. SDA crosslinks are of lower resolution (expected < 25 Å Cα-Cα) compared to the photo-AA crosslinks (expected < 15 Å Cα-Cα) we used on single proteins. The lower resolution poses an additional challenge and the weaker evolutionary signal changes the balance of the data from evolutionary information towards crosslink-based distance restraints, which requires more heavy lifting of the network.

We evaluated AlphaLink on challenging heteromeric CASP15 (Critical Assessment of Structure Prediction[9]) and antibody-antigen targets with simulated crosslinks. Moreover, we validated AlphaLink on in-cell crosslinking MS data[5] from *Bacillus subtilis* that used a different crosslinker, and a virally modified Cullin4-RING ubiquitin ligase (CRL4) complex[10,11]. We focused the evaluation on heteromeric assemblies, since homomers pose a different challenge. The inherent ambiguity of “self” crosslinks in homo-multimeric assemblies rarely permits distinguishing inter- from intra-chain restraints[6].

Integrating crosslinking MS data substantially improves prediction quality of challenging CASP15 targets

AlphaLink with distance restraints vastly outperforms AlphaFold-Multimer[2] on challenging heteromeric CASP15 targets. It achieves similar or better results than the best performing algorithms that participated in CASP15, which used up to 120x more sampling to derive predictions. Integrating simulated SDA crosslinks in the modelling of eight challenging heteromeric CASP15 targets (H1129, H1134, H1140, H1141, H1142, H1144, H1166, H1167) substantially improved the DockQ[12] score from 0.14 to 0.62 on average, compared to the AlphaFold-Multimer baseline (**Fig. 1a**) which matches the average DockQ = 0.62 of the best predictions in CASP15. For comparison, AFSample[13], one of the top performing methods in CASP15, averages a DockQ score of 0.56. Except for H1142, including crosslinking MS data always produced at least acceptable solutions according to DockQ score (DockQ ≥ 0.23[12]). To ensure comparability, we used the same input features as AlphaFold-Multimer (multiple sequence alignments (MSAs) and templates) and fine-tuned AlphaLink on the v2 network weights of AlphaFold-Multimer. Compared to the baseline AlphaFold-Multimer prediction, we increased recycling iterations from 3 to 20 and the number of samples from 25 to 200 (except for H1129 due to computing limitations) to be more in line with methods in CASP15. Increasing sampling and recycling iterations improve the predictions for targets where the crosslinks allow a high degree of flexibility (e.g., H1141) and side chain placement. As a control, **Extended Data Fig. 1** shows AlphaLink outperforming AlphaFold-Multimer with the same recycling iterations = 3 and a comparable number of samples (10 samples for AlphaLink vs 25 for AlphaFold-Multimer).

AlphaLink produced worse predictions than the best groups in CASP15 for three targets (H1129, H1134, H1141). AFsample which uses baseline AlphaFold-Multimer was among the top performers. It demonstrates what is possible with baseline AlphaFold-Multimer with more sampling (up to ~24000 samples for H1166), more recycling (up to 21 iterations), and dropout turned on during inference to create more diverse predictions. This strategy is also compatible with AlphaLink but doesn't scale well with larger complexes since generating large number of samples becomes prohibitively expensive. Predicting a 5900 AA complex (single sample) takes around 30 hours on an NVIDIA A100 GPU with 20 recycling iterations. Crosslinks help to cut down the search space by focusing the sampling on the interesting regions which requires fewer samples.

For H1129, Yang et al. achieved a DockQ over 0.6 by expanding the MSA search and including the monomer predictions as a template. We also noticed that AlphaFold-Multimer predicts chain B of H1129 separately better than within the complex (0.89 vs 0.79), suggesting a potential problem with the fold-and-dock approach of AlphaFold-Multimer and thus AlphaLink which is partially side-stepped by including the monomer prediction as a template. Including the monomer prediction of chain B of H1129 as a template drastically improved the prediction quality (**Extended Data Fig. 2**).

H1134 has only a few contacts in the interface and is more flexible (**Extended Data Fig. 3a**), plausibly explaining the large spread in the DockQ scores in CASP15 (**Extended Data Fig. 3b**). Such flexible targets especially benefit from increased sampling and recycling. In the case of H1134, the model confidence is also less discriminative (**Extended Data Fig. 4**). Crosslinks can improve model selection in this case by selecting first by crosslink satisfaction and second by model confidence (see the accordingly modified AlphaLink* in **Extended Data Fig. 3b**). Training AlphaLink from scratch in the future could improve this by better reflecting crosslinking information in the model confidence.

Originally, in the case of H1141, SDA crosslinks were not restrictive enough (**Extended Data Fig. 1)**. We observe two clusters that differ in the relative orientation of the subunits. Both clusters satisfy all crosslinks (blue in **Extended Data Fig. 5**). However, the better cluster (model confidence 0.86 versus 0.38) corresponds to the crystal structure (DockQ score 0.72). Increasing sampling and recycling helped to select the correct cluster.

The test set comprised both dimers and multimeric assemblies. The simulated crosslink-derived distance restraints had 10% sequence coverage and 20% false-discovery rate[14], resulting in 33 links in the median per protein-protein interaction (including 7 false links, in the median). For comparison purposes, we selected the best predictions based on the highest model confidence[2] (0.8 * interface predicted TM-score (ipTM) + 0.2 * predicted TM-score), which allows us to pick close to the best model (**Extended Data Fig. 6**). Indeed, ipTM and DockQ correlate (ipTM 0.6 equates roughly to DockQ 0.4)[2]. We compare the performance of AlphaLink with and without crosslinks to exclude the influence of other parameters, such as having trained AlphaLink on larger crops than AlphaFold-Multimer v2.2 and the additional fine-tuning. Indeed, we see that the observed improvements are the result of integrating crosslinks (**Extended Data Fig. 7**).

Crosslinking MS data improve modelling of challenging antibody-antigen targets

We extended the evaluation by predicting in addition to CASP15 targets also the interactions of 33 recent antibody-antigen targets from SAbDab[15] (**Fig. 1b)**. Antibody-antigen targets are challenging because the co-evolutionary signal is lower[16]. Here, AlphaLink improves the DockQ on average from 0.29 to 0.6 compared to AlphaFold-Multimer. To limit compute, we used three recycling iterations and five samples for both methods. These results confirm what we have seen for CASP15 where the largest improvements were observed on nanobody-antigen (yellow shaded area in **Fig. 1a**) and antibody-antigen targets (red shaded area in **Fig. 1a**)[16]. In these cases, crosslinking MS data drastically aided prediction. AlphaFold-Multimer models are incorrect for 5 out of 6 targets (DockQ < 0.23[12]) while AlphaLink generates at least medium quality models for 5 out of 6 targets (DockQ > 0.49[12]). Notably, for H1142, H1166, and H1167, AlphaLink produced better median score predictions than the top-ranked CASP15 submissions (**Fig. 1a,c,d**). The DockQ score for H1142 improved from 0.01 for AlphaFold-Multimer and 0.1 in CASP15 to 0.855 by leveraging crosslinking MS data. All true links are satisfied, while 100% of the false links are rejected. This demonstrates a high resilience of AlphaLink towards noise when predicting protein complexes, as was already observed for single proteins[7]. Similarly, the DockQ score for H1166 improved from 0.22 (AlphaFold-Multimer) to 0.8 (AlphaLink), again with crosslink satisfaction and noise rejection being 100%.

A single crosslink obtained in cells can dramatically improve model quality

Encouraged by the success of AlphaLink with simulated data, we modelled 135 dimeric protein-protein interactions (PPIs) with real data[5] from *Bacillus subtilis* cells crosslinked *in situ* with disuccinimidyl sulfoxide (DSSO)[17]. This soluble crosslinker provides restraints between primarily Lys but also Ser, Thr, and Tyr groups. The data are sparse (median 1 crosslink per PPI), however even one crosslink can drastically improve the results (**Fig. 2a**). For example, the model confidence of the CodY-YppF interaction[5,18] improves from 0.25 to 0.81 based on a single crosslink (**Fig. 2b**). For RpoA-RpoC (PDB 6WVK), the DockQ improves from 0.003 to 0.69 based on four in-cell crosslinks (**Fig. 2c**). Each individual crosslink would have sufficed to improve model quality substantially (DockQ 0.69-0.7). We note that changed fine-tuning (larger crops) in AlphaLink2 and AlphaFold-Multimer v2.3 alone leads to some improvements, returning correct models in 5 out of 10 cases for RpoA-RpoC, while adding crosslinks improved this to 10 out of 10.

AlphaLink is fine-tuned on model_1, in comparison, AlphaFold-Multimer predicts the targets with 5 different networks. Using different networks improves the model confidence on average by 0.03 points (**Extended Data Fig. 8).** As seen with the CASP15 targets, crosslinks help to focus sampling on the interesting regions, reducing the amount of sampling required. Overall, integrating crosslinking MS data increases the median model confidence from 0.42 (AlphaFold-Multimer) to 0.6 (AlphaLink). With AlphaLink, 12 additional interactions (total of 46, gain of 35%) reach a model confidence > 0.75. Remarkably, the AlphaLink network was not trained on DSSO data, which differ in linked residues, linker length, and density of data from simulated SDA data. Thus, our results suggest a broad applicability of AlphaLink to varying crosslinker chemistry and the typically low data densities achieved in large-scale and whole-cell crosslinking MS experiments.

AlphaLink reveals the long-enigmatic molecular basis of iron homeostasis in *B. subtilis*

Our recent in-cell crosslinking investigation of protein interactions in *B. subtilis*[5] revealed that the conserved bacterial global regulator for iron homeostasis, Fur, interacts with an essential protein of unknown function, YlaN[18,19]. We confirm here this interaction in a bacterial two-hybrid assay (**Fig. 3a**). In addition, and in agreement with published structures, both Fur[20] and YlaN[21] exhibited self-interaction. Analyses of a Fur-regulated promoter (see **Fig. 3b**) and *in vitro* binding of Fur to the promoter region (**Fig. 3c**) demonstrate that YlaN acts as an antagonist of Fur that prevents it from binding to its DNA targets and thus allows expression of the Fur-repressed genes in the absence of iron (see also **Supplementary Information SI1** for detail). Accordingly, we renamed YlaN to Fpa (Fur protein antagonist). This is corroborated by the observation, that the Fpa knockout is viable if iron(III) is added to the medium[22]. We resorted next to AlphaLink to elucidate the structural basis of Fpa inhibiting Fur. The AlphaLink prediction (model confidence: 0.75) of the *B. subtilis* Fur-dimer (**Fig. 3d**) resembles a V-shaped conformation, similar to other Fur proteins which interact with DNA[20]. AlphaLink predicts a single conformation (model confidence 0.84) consistent with the crosslinking MS data between Lys-74 in the DNA-binding domain of Fur and the Lys residues 23 and 26 of Fpa[5,23] (**Fig. 3d**). This benefited from the integration of crosslinks into the prediction, as AlphaFold-Multimer predicts two conformations for the Fur-Fpa complex, one of which not supporting an interaction (model confidence 0.41). Fpa directly engages the DNA-binding domains of Fur and disassembles the Fur dimerization interface, resulting in a breaking of the functional dimer and a complete re-orientation of the DNA-binding domain (see http://www.subtiwiki.uni-goettingen.de/v4/predictedComplex?id=168 and http://www.subtiwiki.uni-goettingen.de/v4/predictedComplex?id=169 for an interactive display of the Fur dimer and the Fur-Fpa complex as well as **Supplementary Movie MS1**). This structure clearly shows why Fur bound by Fpa is incapable of binding DNA. To verify our AlphaLink model of the Fur-Fpa complex, we tested the interaction of a mutant Fur (Fur*, K18A R23E Y60E) version with Fpa. These surface mutations induce a charge reversal and destroy the salt bridges at different contact points of the binding interface between Fur and Fpa. The Fur* protein showed self-interaction as well as an interaction with the wild type Fur protein. In contrast, no interaction was observed between the mutant Fur* protein and Fpa (see **Fig. 3a**), confirming the predicted AlphaLink model. The proposed rotation and accompanying re-orientation of the DNA-binding domains of Fur explain the loss of the DNA-binding activity of Fur upon interaction with Fpa. Interestingly, the nature of the inducer molecule that causes the release of Fur from DNA in the absence of iron has long been debated. Although direct binding of ferrous iron as a co-repressor has been suggested[24], there is no experimental evidence for such a mechanism. On the contrary, Fur alone binds a promotor in the absence of iron in the buffer (**Fig. 3b**). We show here that it requires the recruitment of the Fur DNA-binding domains by the iron(II)-sensitive Fpa[25] to secure the release of Fur from DNA and thereby iron homeostasis in low iron conditions (**Fig. 3e**).

Crosslinking MS-driven modelling of a multi-protein complex

Finally, we challenged AlphaLink to model, with the help of real sulfo-SDA data, the 6-subunit $CRL4^{DCAF1\text{-}CtD}$/Vpr_{mus}/SAMHD1 assembly[11] (360 kDa, 3118 AA) (**Fig. 4**), using a crystal structure

and cryo-EM density[11] as ground truth. The accessory protein Vpr from certain simian immunodeficiency viruses targets the DCAF1 substrate receptor of host Cullin4-RING ubiquitin ligases (CRL4), to recruit and mark the restriction factor SAMHD1 for proteasomal degradation and thus to stimulate virus replication[11,26]. The v2.2 network weights of AlphaFold-Multimer fail to return meaningful structures of this assembly. This is overcome by moving to v2.3 network weights, which have been trained on larger complexes. Leveraging crosslinks improves the model confidence from 0.56 (AlphaFold-Multimer v2.3) to 0.64 (AlphaLink v2.3) (**Fig. 4a**). The CRL4 subunit CUL4A shows substantial movements, resulting in three conformational states according to cryo-EM data (**Fig. 4b**). AlphaFold-Multimer predicts a contact between CUL4A and DCAF1 that is not supported by the cryo-EM density (**Fig. 4c**). By contrast, AlphaLink predicts no contact (**Fig. 4d**). The density doesn't contain SAMHD1 (shown in light red in **Fig. 4c, d)**. SAMHD1 has both crosslinks to CUL4A (grey) and DDB1 (purple) which influences the arrangement. In addition, crosslinks allow AlphaLink to position the viral Vpr protein inside the experimental density in agreement with the crystal structure (PDB 6ZX9) (**Fig. 4e, green, f**), while AlphaFold-Multimer places Vpr incorrectly. Our predicted Vpr-DCAF1 interaction model achieved a DockQ score of 0.56 compared to 0.04 by AlphaFold-Multimer (**Fig. 4f**).

Conclusion

Our findings demonstrate the successful extension of AlphaLink, an experiment-assisted AI approach, to predict protein complex structures. We can now start visualising at pseudo-atomic resolution protein-protein interactions inside cells, by leveraging the very scarce data of whole-cell crosslinking MS. With this breakthrough, protein-protein interaction studies move from delivering links (who) to structures (how), inside cells and at scale. Importantly, in-cell crosslinking reveals protein interactions that are often lost upon cell lysis[5]. While lysis is required frequently for large-scale study of protein complexes, doing so without prior crosslinking challenges especially transient and fragile features of complexes. AlphaLink with whole-cell crosslinking will therefore accelerate discovering hitherto hidden aspects of biology, to advance our understanding of life and widen our therapeutic options in cases of disease.

References

1. Jumper, J. *et al.* Highly accurate protein structure prediction with AlphaFold. *Nature* **596**, 583–589 (2021).
2. Evans, R. *et al.* Protein complex prediction with AlphaFold-Multimer. *bioRxiv* 2021.10.04.463034 (2022) doi:10.1101/2021.10.04.463034.
3. Tang, X. & Bruce, J. E. Chemical Cross-Linking for Protein–Protein Interaction Studies. in *Mass Spectrometry of Proteins and Peptides: Methods and Protocols* (eds. Lipton, M. S. & Paša-Tolic, L.) 283–293 (Humana Press, 2009).
4. Lenz, S. *et al.* Reliable identification of protein-protein interactions by crosslinking mass spectrometry. *Nat. Commun.* **12**, 3564 (2021).
5. O'Reilly, F. J. *et al.* Protein complexes in cells by AI-assisted structural proteomics. *Mol. Syst. Biol.* **19**, e11544 (2023).
6. Maiolica, A. *et al.* Structural analysis of multiprotein complexes by cross-linking, mass spectrometry, and database searching. *Mol. Cell. Proteomics* **6**, 2200–2211 (2007).
7. Stahl, K., Graziadei, A., Dau, T., Brock, O. & Rappsilber, J. Protein structure prediction with in-cell photo-crosslinking mass spectrometry and deep learning. *Nat. Biotechnol.* (2023) doi:10.1038/s41587-023-01704-z.
8. Belsom, A., Schneider, M., Fischer, L., Brock, O. & Rappsilber, J. Serum Albumin Domain Structures in Human Blood Serum by Mass Spectrometry and Computational Biology. *Mol. Cell. Proteomics* **15**, 1105–1116 (2016).
9. Moult, J., Pedersen, J. T., Judson, R. & Fidelis, K. A large-scale experiment to assess protein structure prediction methods. *Proteins* **23**, ii–v (1995).
10. Mahon, C., Krogan, N. J., Craik, C. S. & Pick, E. Cullin E3 ligases and their rewiring by viral factors. *Biomolecules* **4**, 897–930 (2014).
11. Banchenko, S. *et al.* Structural insights into Cullin4-RING ubiquitin ligase remodelling by Vpr from simian immunodeficiency viruses. *PLoS Pathog.* **17**, e1009775 (2021).
12. Basu, S. & Wallner, B. DockQ: A Quality Measure for Protein-Protein Docking Models. *PLoS One* **11**, e0161879 (2016).
13. Wallner, B. AFsample: improving multimer prediction with AlphaFold using massive sampling. *Bioinformatics* **39**, (2023).
14. Fischer, L. & Rappsilber, J. Quirks of Error Estimation in Cross-Linking/Mass Spectrometry. *Anal. Chem.* **89**, 3829–3833 (2017).
15. Dunbar, J. *et al.* SAbDab: the structural antibody database. *Nucleic Acids Res.* **42**, D1140–6 (2014).
16. Yin, R., Feng, B. Y., Varshney, A. & Pierce, B. G. Benchmarking AlphaFold for protein complex modeling reveals accuracy determinants. *Protein Sci.* **31**, e4379 (2022).
17. Kao, A. *et al.* Development of a novel cross-linking strategy for fast and accurate identification of cross-linked peptides of protein complexes. *Mol. Cell. Proteomics* **10**, M110.002212 (2011).
18. Pedreira, T., Elfmann, C. & Stülke, J. The current state of SubtiWiki, the database for the model organism Bacillus subtilis. *Nucleic Acids Res.* **50**, D875–D882 (2022).
19. Wicke, D., Meißner, J., Warneke, R., Elfmann, C. & Stülke, J. Understudied proteins and understudied functions in the model bacterium Bacillus subtilis—A major challenge in

current research. *Mol. Microbiol.* **120**, 19–18 (2023).
20. Butcher, J., Sarvan, S., Brunzelle, J. S., Couture, J.-F. & Stintzi, A. Structure and regulon of Campylobacter jejuni ferric uptake regulator Fur define apo-Fur regulation. *Proc. Natl. Acad. Sci. U. S. A.* **109**, 10047–10052 (2012).
21. Xu, L. *et al.* Crystal structure of S. aureus YlaN, an essential leucine rich protein involved in the control of cell shape. *Proteins* **68**, 438–445 (2007).
22. Peters, J. M. *et al.* A Comprehensive, CRISPR-based Functional Analysis of Essential Genes in Bacteria. *Cell* **165**, 1493–1506 (2016).
23. Elfmann, C. & Stülke, J. PAE viewer: a webserver for the interactive visualization of the predicted aligned error for multimer structure predictions and crosslinks. *Nucleic Acids Res.* **51**, W404–W410 (2023).
24. Lee, J.-W. & Helmann, J. D. Functional specialization within the Fur family of metalloregulators. *Biometals* **20**, 485–499 (2007).
25. Boyd, J. M. *et al.* YlaN is an iron(II) binding protein that functions to relieve Fur-mediated repression of gene expression in Staphylococcus aureus. *bioRxiv* 2023.10.03.560778 (2023) doi:10.1101/2023.10.03.560778.
26. Fregoso, O. I. *et al.* Evolutionary toggling of Vpx/Vpr specificity results in divergent recognition of the restriction factor SAMHD1. *PLoS Pathog.* **9**, e1003496 (2013).
27. Vallat, B., Webb, B., Westbrook, J. D., Sali, A. & Berman, H. M. Development of a Prototype System for Archiving Integrative/Hybrid Structure Models of Biological Macromolecules. *Structure* **26**, 894–904.e2 (2018).
28. Kahraman, A., Malmström, L. & Aebersold, R. Xwalk: computing and visualizing distances in cross-linking experiments. *Bioinformatics* **27**, 2163–2164 (2011).
29. Li, Z. *et al.* Uni-Fold: An Open-Source Platform for Developing Protein Folding Models beyond AlphaFold. *bioRxiv* 2022.08.04.502811 (2022) doi:10.1101/2022.08.04.502811.
30. Ahdritz, G. *et al.* OpenFold: Retraining AlphaFold2 yields new insights into its learning mechanisms and capacity for generalization. *bioRxiv* 2022.11.20.517210 (2022) doi:10.1101/2022.11.20.517210.
31. Townshend, R., Bedi, R., Suriana, P. & Dror, R. End-to-end learning on 3d protein structure for interface prediction. *Adv. Neural Inf. Process. Syst.* **32**, (2019).
32. Leemann, M. *et al.* Automated benchmarking of combined protein structure and ligand conformation prediction. *Proteins* **91**, 1912–1924 (2023).
33. Méndez, R., Leplae, R., De Maria, L. & Wodak, S. J. Assessment of blind predictions of protein-protein interactions: current status of docking methods. *Proteins* **52**, 51–67 (2003).
34. Sambrook, J., Fritsch, E. F., Maniatis, T. & Others. *Molecular cloning: a laboratory manual*. (Cold spring harbor laboratory press, 1989).
35. Kunst, F. & Rapoport, G. Salt stress is an environmental signal affecting degradative enzyme synthesis in Bacillus subtilis. *J. Bacteriol.* **177**, 2403–2407 (1995).
36. Schmalisch, M. H., Bachem, S. & Stülke, J. Control of the Bacillus subtilis antiterminator protein GlcT by phosphorylation. Elucidation of the phosphorylation chain leading to inactivation of GlcT. *J. Biol. Chem.* **278**, 51108–51115 (2003).
37. Diethmaier, C. *et al.* A novel factor controlling bistability in Bacillus subtilis: the YmdB protein affects flagellin expression and biofilm formation. *J. Bacteriol.* **193**, 5997–6007 (2011).

38. Schirmer, F., Ehrt, S. & Hillen, W. Expression, inducer spectrum, domain structure, and function of MopR, the regulator of phenol degradation in Acinetobacter calcoaceticus NCIB8250. *J. Bacteriol.* **179**, 1329–1336 (1997).
39. Martin-Verstraete, I., Débarbouillé, M., Klier, A. & Rapoport, G. Interactions of wild-type and truncated LevR of Bacillus subtilis with the upstream activating sequence of the levanase operon. *J. Mol. Biol.* **241**, 178–192 (1994).
40. Weinrauch, Y., Msadek, T., Kunst, F. & Dubnau, D. Sequence and properties of comQ, a new competence regulatory gene of Bacillus subtilis. *J. Bacteriol.* **173**, 5685–5693 (1991).
41. Pietack, N. *et al.* In vitro phosphorylation of key metabolic enzymes from Bacillus subtilis: PrkC phosphorylates enzymes from different branches of basic metabolism. *J. Mol. Microbiol. Biotechnol.* **18**, 129–140 (2010).
42. Bradford, M. M. A rapid and sensitive method for the quantitation of microgram quantities of protein utilizing the principle of protein-dye binding. *Anal. Biochem.* **72**, 248–254 (1976).
43. Karimova, G., Pidoux, J., Ullmann, A. & Ladant, D. A bacterial two-hybrid system based on a reconstituted signal transduction pathway. *Proc. Natl. Acad. Sci. U. S. A.* **95**, 5752–5756 (1998).

Acknowledgements

We thank Andrea Graziadei and David Schwefel for their feedback on the manuscript and David Schwefel for helping to identify potential mutations. We are grateful to the Uni-Fold team for providing a fully open-source and trainable reimplementation of AlphaFold-Multimer (https://github.com/dptech-corp/Uni-Fold).

Funding

This research was supported by the Wellcome Trust [Grant number 227166] (JR, KS) and the Deutsche Forschungsgemeinschaft (DFG, German Research Foundation) under Germany´s Excellence Strategy – EXC 2008 – 390540038 (JR) – UniSysCat (JR) and under Germany's Excellence Strategy – EXC 2002/1 "Science of Intelligence" – project number 390523135 (OB). The Wellcome Centre for Cell Biology is supported by core funding from the Wellcome Trust [203149]. For the purpose of open access, the author has applied a CC BY public copyright licence to any Author Accepted Manuscript version arising from this submission. Deutsche Forschungsgemeinschaft (DFG, German Research Foundation) [Grant number 469281184] (JS).

Author contributions

Software development: KS

Data Analysis: KS, LD, RB, RW, BH

Supervision: JR, OB, JS

Supplement information: LD, RB, RW, BH, JS

Writing- initial draft: KS, JR, OB

Writing- editing and revision: KS, JR, OB, LD, RB, RW, BH, JS

Competing interests

The other authors declare no competing interests.

Data and materials availability

AlphaLink models based on experimental crosslinks have been deposited as integrative/hybrid models in PDB-Dev[27] with accession codes PDBDEV_00000221 and PDBDEV_G_1000003.
The code for AlphaLink is deposited at https://github.com/Rappsilber-Laboratory/AlphaLink2.
Model weights were deposited at Zenodo: doi:10.5281/zenodo.8007238

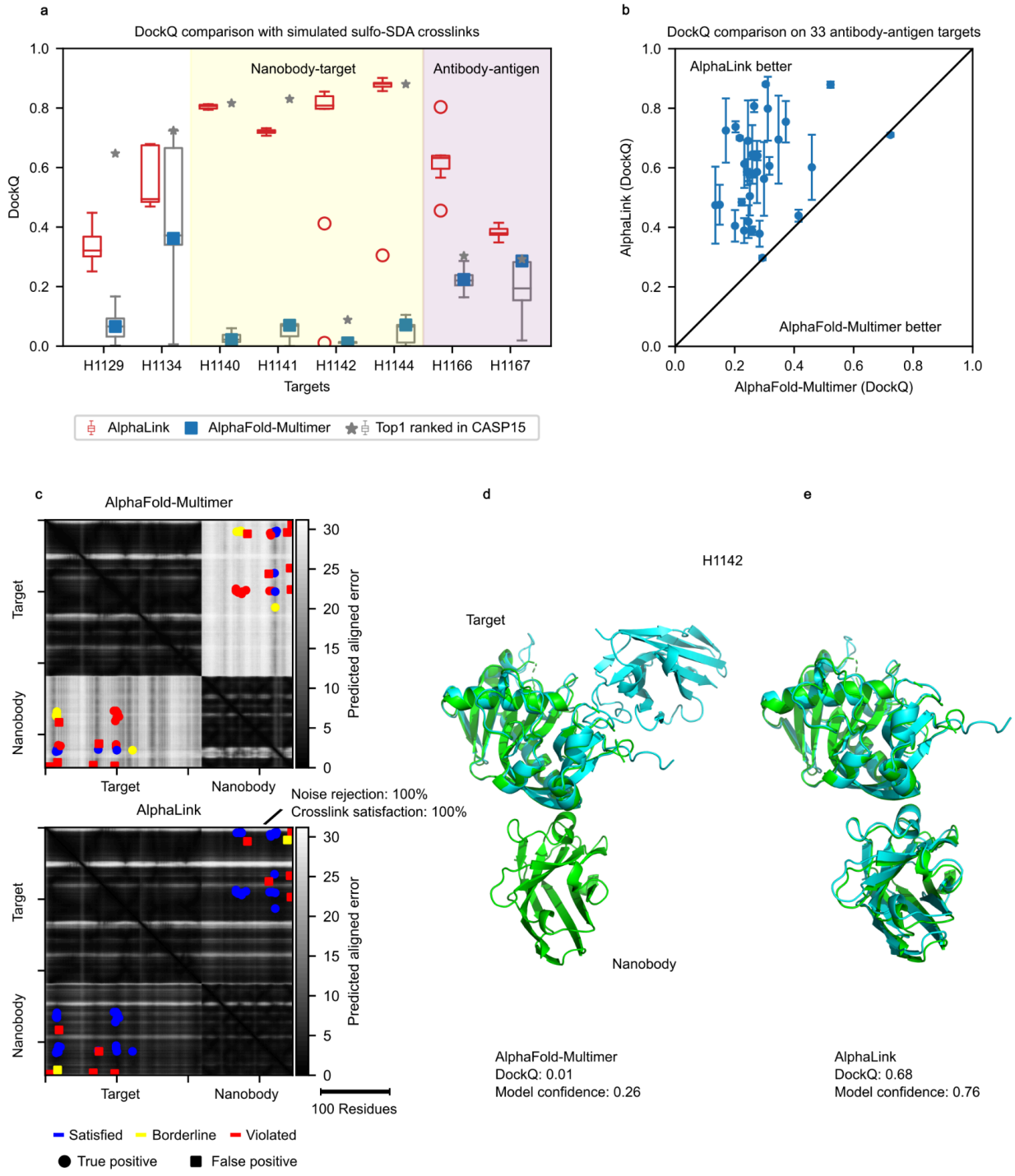

Fig. 1: AlphaLink performance on simulated data.

a- DockQ comparison on 8 heteromeric CASP15 targets with simulated SDA crosslinks. The AlphaLink boxplot shows the highest model confidence model (N = 200) for 10 randomly sampled crosslink sets. The top ranked predictions (grey) correspond to all submissions that

were ranked first by the participants (model_1), the best for each target is highlighted with an asterisk. AlphaFold-Multimer is highlighted in blue (model_1). The yellow shaded area highlights nanobody, and the red shaded area antibody targets. In all boxplots, the line shows the median and the whiskers represent the 1.5x interquartile range. **b-** DockQ comparison of AlphaLink and AlphaFold-Multimer on 33 antibody-antigen targets from SAbDab. **c-** PAE map comparison of AlphaFold-Multimer and AlphaLink for H1142. **d-** AlphaFold-Multimer prediction for H1142 (cyan) aligned to the crystal structure (green). **e-** AlphaLink prediction for H1142 (cyan) aligned to the crystal structure (green). The red circle highlights differences in side chain orientations in the interface.

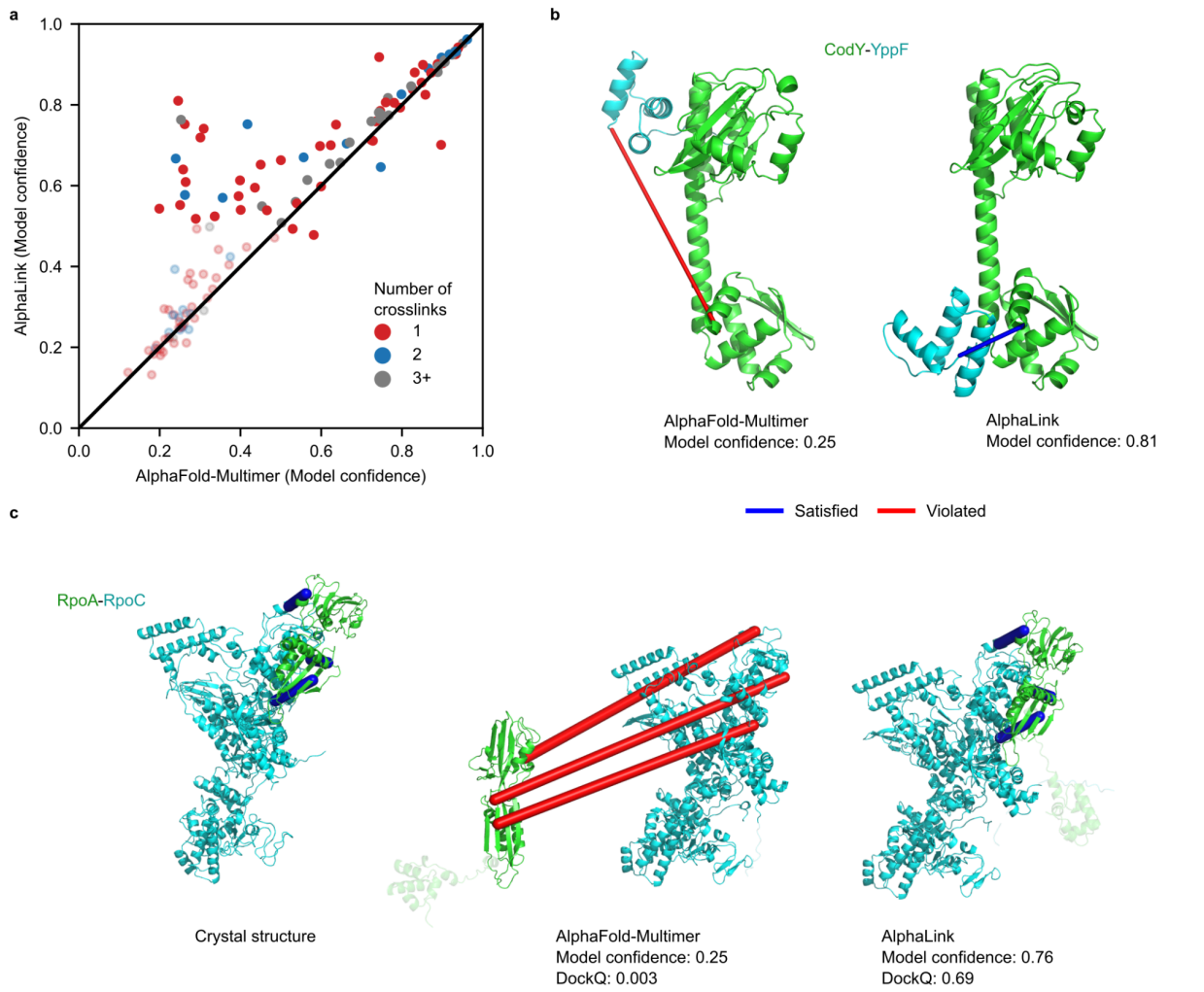

Fig. 2: AlphaLink performance on real data from *Bacillus subtilis*.
a- Highest model confidence of AlphaLink v2.2 (N = 5) vs AlphaFold-Multimer v2.2 (M = 5) on the *Bacillus subtilis* data on K = 135 dimeric protein-protein interactions. Low confidence predictions for both methods (model confidence < 0.5) have higher transparency. **b-** AlphaFold-Multimer (left) and AlphaLink (right) prediction for CodY-YppF with annotated crosslinks (blue - satisfied, red - violated). **c-** Comparison of crystal structure (left), AlphaFold-Multimer prediction (middle) and AlphaLink prediction (right) for RpoA-RpoC with annotated crosslinks (blue - satisfied, red - violated). We omitted one crosslink that is not covered by the crystal structure.

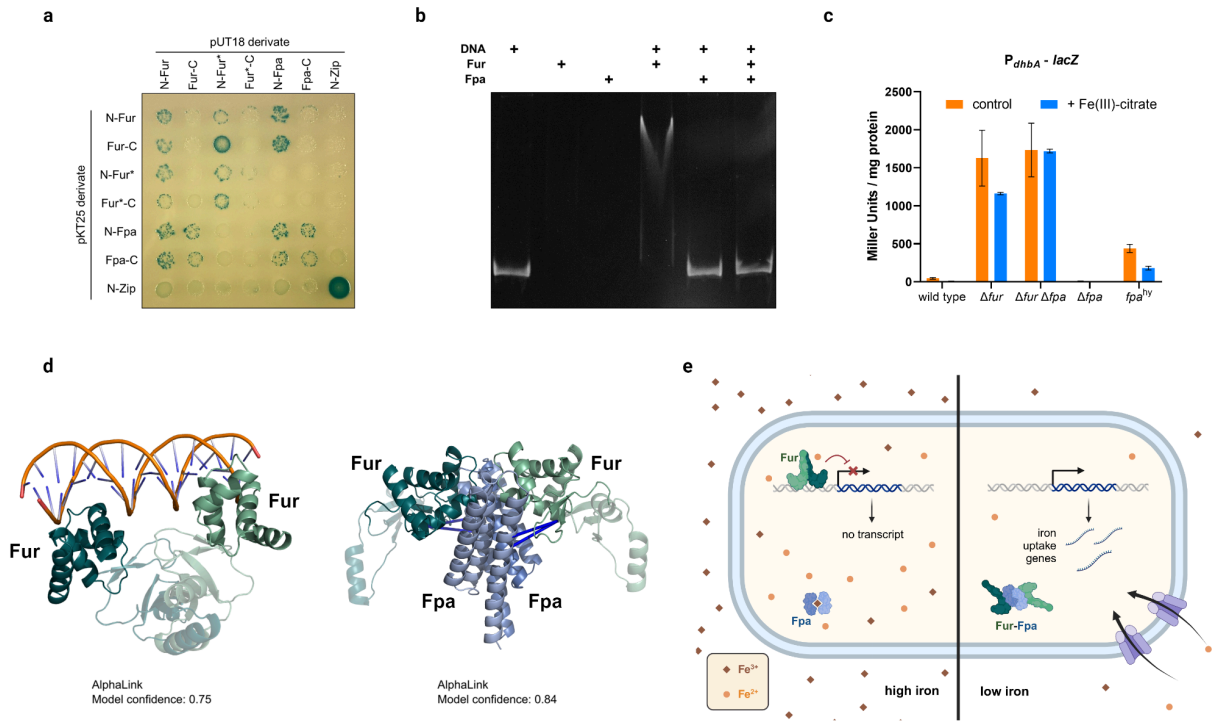

Fig. 3: The Fpa-Fur interaction controls iron homeostasis in *B. subtilis*. **a-** Bacterial two-hybrid assay to test the interaction between Fur and Fpa. N- and C-terminal fusions of both proteins as well as the mutant Fur* protein to the T18 or T25 domain of the adenylate cyclase (CyaA) were created and the proteins were tested for interaction in *E. coli* BTH101. Blue colonies indicate an interaction that results in adenylate cyclase activity and subsequent expression of the reporter β-galactosidase. **b-** Gel electrophoretic mobility shift assay of Fur binding to *dhbA* promoter fragments in the absence of iron. The components added to the assays are shown above the gels. **c-** The impact of Fpa on *dhbA* promoter activity. Strains carrying a *dhbA-lacZ* fusion were cultivated in LB with or without added ferric citrate, and promoter activities were determined by quantification of b-galactosidase activities. The values are averages of three independent experiments. Standard deviations are shown. **d-** AlphaLink predicts the structure of the Fur-Fpa complex. Left: AlphaLink prediction (model confidence: 0.75) of the Fur dimer. Right: AlphaLink prediction (model confidence: 0.84) of the Fpa-Fur complex with crosslinking MS data. The Fur dimer undergoes a large conformational change. The dimerization region is shown in transparent. All crosslinks (shown as blue lines) are satisfied in the prediction. **e-** Model for the control of Fur activity by Fpa. At high iron concentrations, the Fur dimer binds its target DNA sequences in the promoter regions of genes involved in iron homeostasis. The Fpa protein binds ferrous iron and is unable to interact with Fur. If iron gets limiting, apo-Fpa forms a complex with Fur, resulting in the release of Fur from its DNA targets, and thus in expression of genes for iron uptake.

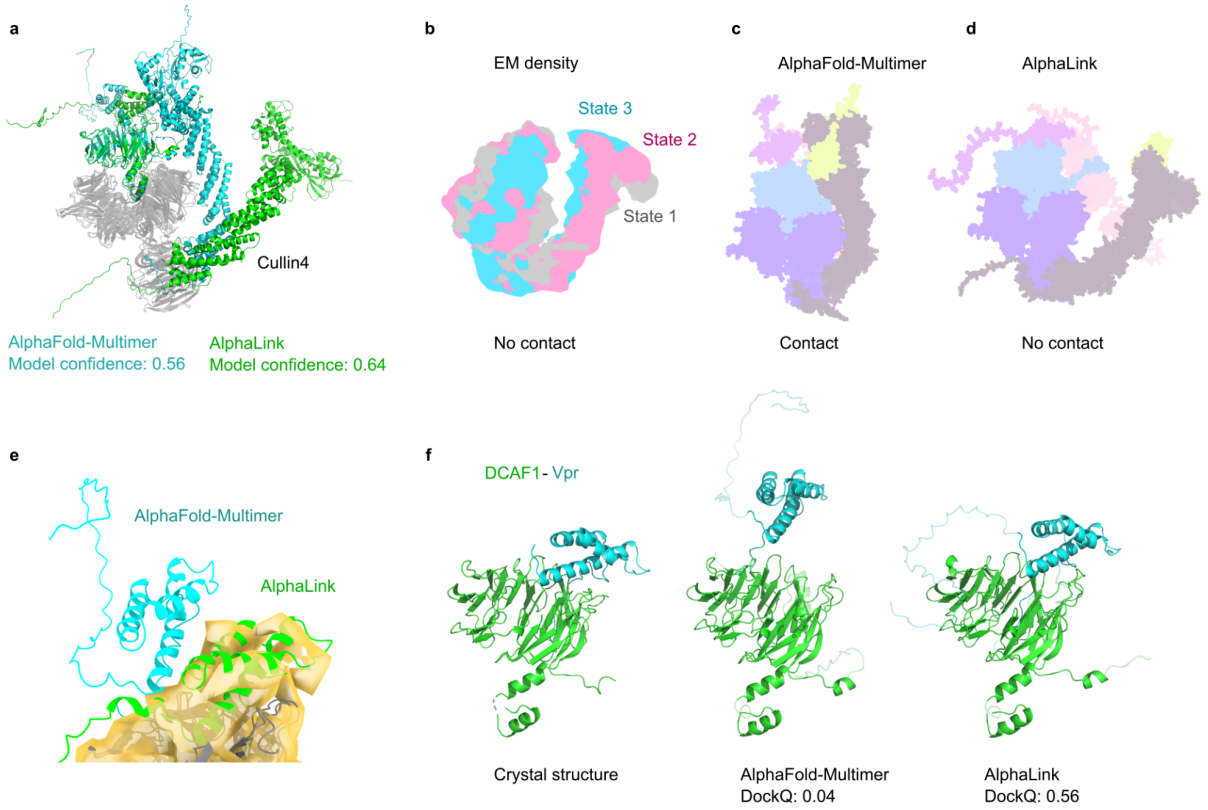

Fig. 4: AlphaLink performance on real data from CRL4 with v2.3 weights.
a- AlphaFold-Multimer (v2.3) (cyan) and AlphaLink (v2.3) (green) prediction for a virally modified CRL4 assembly. SAMHD1 is not visualised for clarity. **b-** Schematic view of the three states of Cullin4 observed in the EM density (EMD-10612 to EMD-10614). SAMHD1 is not part of the density. **c-** Schematic view of the AlphaFold-Multimer prediction, showing a contact not present in the density (**b**). **d-** Schematic view of the AlphaLink prediction. SAMHD1 is shown in light red. **e-** Placement of the viral Vpr protein for AlphaFold-Multimer (cyan) and AlphaLink (green) in the EM density. **f-** Predictions of DCAF1-Vpr compared to the crystal structure (PDB 6ZX9).

Supplementary Materials

Materials and Methods

Crosslink simulation. We simulate SDA crosslinks with XWalk[28] with a 25 Å Cα-Cα cutoff and trypsin digestion. We add FDR=20% of noise to match the expected FDR. At least one crosslink is always incorrect, the actual FDR can therefore be much higher. False positive crosslinks can be any residue pair > 25 Å Cα-Cα, where one residue is a Lys, Ser, Thr, and Tyr. In real data, there is often an affinity towards Lys and clustering of crosslinks. These biases are not reflected in the simulation since we uniformly subsample the crosslink candidates. This doesn't play a big role in training and we can see that it translates to real data but it may give a better coverage during testing than what we can normally expect. The link-level FDR is simulated by shuffling the crosslinks and counting the number of incorrect links observed so far. The coverage is set to 10% and corresponds to the sequence coverage based on the longer sequence. We sample inter- and intra-protein crosslinks independently.

Integration of crosslinks. We integrate crosslinks in AlphaLink[7] the same way we did in the monomer version. We add a crosslink embedding layer to the neural network that projects the soft label contact map into the 128-d z-space. The projection is added to the pair representation (z). This way, the crosslinking information influences retrieval of the co-evolutionary information and the coupled updates with the MSA representation enables noise rejection.

Fine-tuning of AlphaFold-Multimer. We switched to Uni-Fold[29] since OpenFold[30] didn't support multimers. To avoid training Uni-Fold from scratch, we fine-tune the weights provided by Deepmind. For v2 we use AlphaFold-Multimer 2.2.4 weights as the starting point (https://github.com/deepmind/alphafold/releases/tag/v2.2.4). AlphaFold-Multimer was trained on PDBs deposited before 2018-04-30, predating CASP13. For v3, we use the AlphaFold-Multimer 2.3.0 weights (https://github.com/deepmind/alphafold/releases/tag/v2.3.0). AlphaFold-Multimer was trained on PDBs deposited before 2021-09-30, predating CASP15. The networks are refined on 11424 protein complexes with a total of 34054 chains from the DIPS-Plus[31] training set with simulated SDA crosslinking data. DIPS-Plus contains PDBs deposited before May 2021, predating CASP15. We use Uni-Fold v2.1.0 (https://github.com/dptech-corp/Uni-Fold/releases/tag/v2.1.0). MSAs were generated with the reduced database setting. We train and test with model_1. Since we focus on heteromers, we sample homomeric crosslinks like heteromeric crosslinks during training to have more samples.

For training, we follow the refinement training regime outlined in the AlphaFold-Multimer paper but expand the crop size to 640AA to increase interface exposure and the number of crosslinks we see during training. We train on 4 A100 GPUs for 10 days. We used early stopping on the validation set which consists of proteins from CAMEO[32] released after 2022.

Evaluation set up. For the comparison, we use the official predictions from CASP15. Our main comparison point is NBIS-AF2-multimer which corresponds to standard AlphaFold-Multimer v2.

We use the same MSAs as NBIS-AF2-multimer provided by Arne Elofsson (http://duffman.it.liu.se/casp15/). We increased the recycling iterations to 20, the original comparison can be found in **Extended Fig. 1**. We randomly sample 10 crosslink sets with 10% coverage and 20% FDR for each target and predict each with a different seed for a total of 200 seeds (10 in the original comparison). We only relax the best sample (chosen by model confidence) per crosslink set. The maximum MSA cluster size is 512 sequences.
For the SAbDab comparison, we compile a new data set consisting of 33 recent antibody-antigen targets between 01-01-2022 and 11-10-2023 which represent challenging protein complexes due to the lower evolutionary signal. We only include targets which have a crystal structure with a resolution of 3 Å or better and a single assembly, to simplify the evaluation.

The primary evaluation metric is the DockQ score. We compute the DockQ scores for AlphaLink with the official CASP15 evaluation scripts (https://git.scicore.unibas.ch/schwede/casp15_ema).

The DockQ score is the average of the fraction of native contacts (F_{nat}), the interface RMSD (iRMS)[33], and the ligand RMSD (LRMS)[33]. The interface includes all contacting residues. Residues are in contact if they are from different chains and at least one heavy atom is within 5 Å. The iRMS increases the cutoff to 10 Å. The F_{nat} then corresponds to the recall of the native contacts. The iRMS is the RMSD of the backbone atoms in the interface. The LRMS is the RMSD after superimposing the larger of the two structures onto the smaller one. The final DockQ score is the average DockQ score over all interfaces for protein complexes with more than two chains.

We only relax the best prediction per crosslink subset to save compute time. Relaxing only slightly changes the final scores.

For the *Bacillus subtilis* predictions, we use the same MSAs as O'Reilly et al.[5]. We predict the targets again with AlphaFold-Multimer v2.2 to be comparable. The results with the original AlphaFold-Multimer v2.1 predictions from the study are shown in **Extended Data Fig. 9**. The model confidence might not be comparable. Except for few targets, there are no crystal structures available for Bacillus subtilis which is why we have to resort to model confidence as an indicator of improvement. **Extended Data Fig. 10a** shows the correlation between the model confidence and the DockQ score and further the relationship between the model confidences of AlphaLink and AlphaFold-Multimer in respect to the DockQ score (**Extended Fig. 10b**). Although, on these hard targets, the model confidence is an overestimation, a better model confidence generally translates into a better DockQ score.

For the Cullin4 complex, we use the v3 weights to predict the structures. We always predict the full complex and use the same MSAs for both AlphaFold-Multimer and AlphaLink. We compare the prediction of DCAF1-Vpr to the crystal structure (PDB 6ZX9) with the T4 tag removed. The EM densities correspond to the EMDB (https://www.ebi.ac.uk/pdbe/emdb/) accession codes: EMD-10611 (core), EMD-10612 (conformational state-1), EMD-10613 (state-2) and EMD-10614 (state-3).

Strains, media and growth conditions. *E. coli* DH5α and Rosetta DE3 (28) were used for cloning and for the expression of recombinant proteins, respectively. All *B. subtilis* strains used in this study are derivatives of the laboratory strain 168. They are listed in **Supplementary**

Table S1. *B. subtilis* and *E. coli* were grown in Luria-Bertani (LB) or in sporulation (SP) medium[34,35]. For growth assays and the *in vivo* interaction experiments, *B. subtilis* was cultivated in LB, SP, or CSE-Glc minimal medium[35,36]. CSE-Glc is a chemically defined medium that contains sodium succinate (6 g/l), potassium glutamate (8 g/l), and glucose (1 g/l) as the carbon sources[36]. Iron sources were added as indicated. The media were supplemented with ampicillin (100 µg/ml), kanamycin (50 µg/ml), chloramphenicol (5 µg/ml), or erythromycin and lincomycin (2 and 25 µg/ml, respectively) if required. LB and SP plates were prepared by the addition of Bacto Agar (Difco) (17 g/l) to the medium.

DNA manipulation. Transformation of *E. coli* and plasmid DNA extraction were performed using standard procedures[34]. All commercially available plasmids, restriction enzymes, T4 DNA ligase and DNA polymerases were used as recommended by the manufacturers. *B. subtilis* was transformed with plasmids, genomic DNA or PCR products according to the two-step protocol[35]. Transformants were selected on SP plates containing erythromycin (2 µg/ml) plus lincomycin (25 µg/ml), chloramphenicol (5 µg/ml), kanamycin (10 µg/ml), or spectinomycin (250 µg/ml). DNA fragments were purified using the QIAquick PCR Purification Kit (Qiagen, Hilden, Germany). DNA sequences were determined by the dideoxy chain termination method[34].

Construction of mutant strains by allelic replacement. Deletion of the *fur* and *fpa* genes was achieved by transformation of *B. subtilis* 168 or GP879 with a PCR product constructed using oligonucleotides to amplify DNA fragments flanking the target genes and an appropriate intervening resistance cassette as described previously[37]. The integrity of the regions flanking the integrated resistance cassette was verified by sequencing PCR products of about 1,100 bp amplified from chromosomal DNA of the resulting mutant strains.

Phenotypic analysis. In *B. subtilis*, amylase activity was detected after growth on plates containing nutrient broth (7.5 g/l), 17 g Bacto agar/l (Difco) and 5 g hydrolyzed starch/l (Connaught). Starch degradation was detected by sublimating iodine onto the plates.

Quantitative studies of *lacZ* expression in *B. subtilis* were performed as follows: cells were grown in CSE-Glc or LB medium supplemented with iron sources as indicated. Cells were harvested at OD600 of 0.5 to 0.8. b-Galactosidase specific activities were determined with cell extracts obtained by lysozyme treatment as described previously[35]. One unit of b-galactosidase is defined as the amount of enzyme which produces 1 nmol of o-nitrophenol per min at 28° C.

Plasmid constructions. To express the Fur and Fpa proteins carrying a N-terminal His-tag in *E. coli*, the *fur* and *fpa* genes were amplified using chromosomal DNA of *B. subtilis* 168 as the template and appropriate oligonucleotides that attached specific restriction sites to the fragment. Those were: BamHI and XhoI for cloning *fur* in pET-SUMO (Invitrogen, Germany), and BamHI and SalI for cloning *fpa* in pWH844[38]. The resulting plasmids were pGP3589 and pGP2583 for Fur and Fpa, respectively.

For overexpression of *fpa* in *B. subtilis*, we constructed plasmid pGP3897. For this purpose, the *fpa* gene was amplified and cloned between the BamHI and SalI site of the expression vector pBQ200[39].

Plasmid pAC7[40] was used to construct a translational fusion of the *dhbA* promoter region to the promoterless *lacZ* gene. For this purpose, the promoter region was amplified using oligonucleotides that attached EcoRI and BamHI restriction to the ends of the products. The fragments were cloned between the EcoRI and BamHI sites of pAC7. The resulting plasmid was pGP3594.

Protein expression and purification. *E. coli* Rosetta(DE3) was transformed with the plasmid pGP371[41], pGP2583, and pGP3589 encoding His-tagged versions of PtsH, Fpa, and Fur, respectively. For overexpression, cells were grown in 2x LB and expression was induced by the addition of isopropyl 1-thio-β-D-galactopyranoside (final concentration, 1 mM) to exponentially growing cultures (OD_{600} of 0.8). The His-tagged proteins were purified in 1x ZAP buffer (50 mM Tris-HCl, 200 mM NaCl, pH 7.5). Cells were lysed by four passes (18,000 p.s.i.) through an HTU DIGI-F press (G. Heinemann, Germany). After lysis, the crude extract was centrifuged at 46,400 x g for 60 min and then passed over a Ni^{2+}nitrilotriacetic acid column (IBA, Göttingen, Germany). The proteins were eluted with an imidazole gradient. After elution, the fractions were tested for the desired protein using SDS-PAGE. The purified proteins were concentrated in a Vivaspin turbo 15 (Sartorius) centrifugal filter device (cut-off 5 or 50 kDa). The protein samples were stored at −80°C until further use. The protein concentration was determined according to the method of Bradford[42] using the Bio-Rad dye binding assay and bovine serum albumin as the standard.

Electromobility shift assay (EMSA) with DNA. To analyze the binding of Fur to the *dhbA* promoter region, we performed EMSA assays with a 284 bp *dhbA* promoter fragment that carries the Fur binding site and purified Fur, Fpa, and PtsH proteins. 200 ng of DNA and 80 pmol of the proteins were used. The samples were first prepared without the proteins only with DNA, buffer and water and heated for 2 minutes at 95°C. Then the proteins were added in different combinations and the samples were incubated for 30 minutes at 37°C. Meanwhile, the EMSA gels were applied to a pre run at 90 V for 30 minutes immersed in TBE buffer (28). Afterwards, 2 µl of the loading dye were added and the samples were loaded into the gel pockets. The gel was run for 3 hours at 110 V. Then, the gels were immersed in TBE containing HDGreen® fluoreszence dye (Intas, Germany). After 2 minutes the gels were photographed under UV light.

Bacterial two-hybrid assay. Primary protein-protein interactions were identified by bacterial two-hybrid (BACTH) analysis[43]. The BACTH system is based on the interaction-mediated reconstruction of *Bordetella pertussis* adenylate cyclase (CyaA) activity in *E. coli* BTH101. Functional complementation between two fragments (T18 and T25) of CyaA as a consequence of the interaction between bait and prey molecules results in the synthesis of cAMP, which is monitored by measuring the β-galactosidase activity of the cAMP-CAP-dependent promoter of the *E. coli lac* operon. Plasmids pUT18C and p25N allow the expression of proteins fused to the T18 and T25 fragments of CyaA, respectively. For these experiments, we used the plasmids pGP3868-pGP3875, which encode N-and C-terminal fusions of T18 or T25 to *fur* and *fpa.* The plasmids were obtained by cloning the *fur* and *fpa* between the KpnI and BamHI sites of pUT18C and p25N[43]. The mutant *fur** allele was purchased from Eurofins Genomics (Germany)

and then amplified and cloned as the wild type *fur* gene. The resulting plasmids were then used for co-transformation of *E. coli* BTH101 and the protein-protein interactions were then analysed by plating the cells on LB plates containing 100 µg/ml ampicillin, 50 µg/ml kanamycin, 40 µg/ml X-Gal (5-bromo-4-chloro-3-indolyl-ß-D-galactopyranoside), and 0.5 mM IPTG (isopropyl-ß-D-thiogalactopyranoside). The plates were incubated for a maximum of 36 h at 28°C.

Supplementary Table S1. *B. subtilis* strains used in this study.

Strain	Genotype	Source or Reference
168	*trpC2*	Laboratory collection
GP879	*trpC2* Δ*fur*::*ermC*	This study
GP3321	*trpC2* Δ*fur*::*ermC* Δ*fpa*::*cat*	This study
GP3324	*trpC2* Δ*fpa*::*cat*	This study
GP3331	*trpC2 amyE*::(P_{dhbA}-*lacZ aphA3*)	pGP3594 → 168
GP3356	*trpC2* Δ*fur*::*ermC amyE*::(P_{dhbA}-*lacZ aphA3*)	GP879 → GP3331
GP3361	*trpC2* Δ*fur*::*ermC* Δ*fpa*::*cat amyE*::(P_{dhbA}-*lacZ aphA3*)	GP3321 → GP3331
GP3366	*trpC2* Δ*fpa*::*cat amyE*::(P_{dhbA}-*lacZ aphA3*)	GP3324 → GP3331

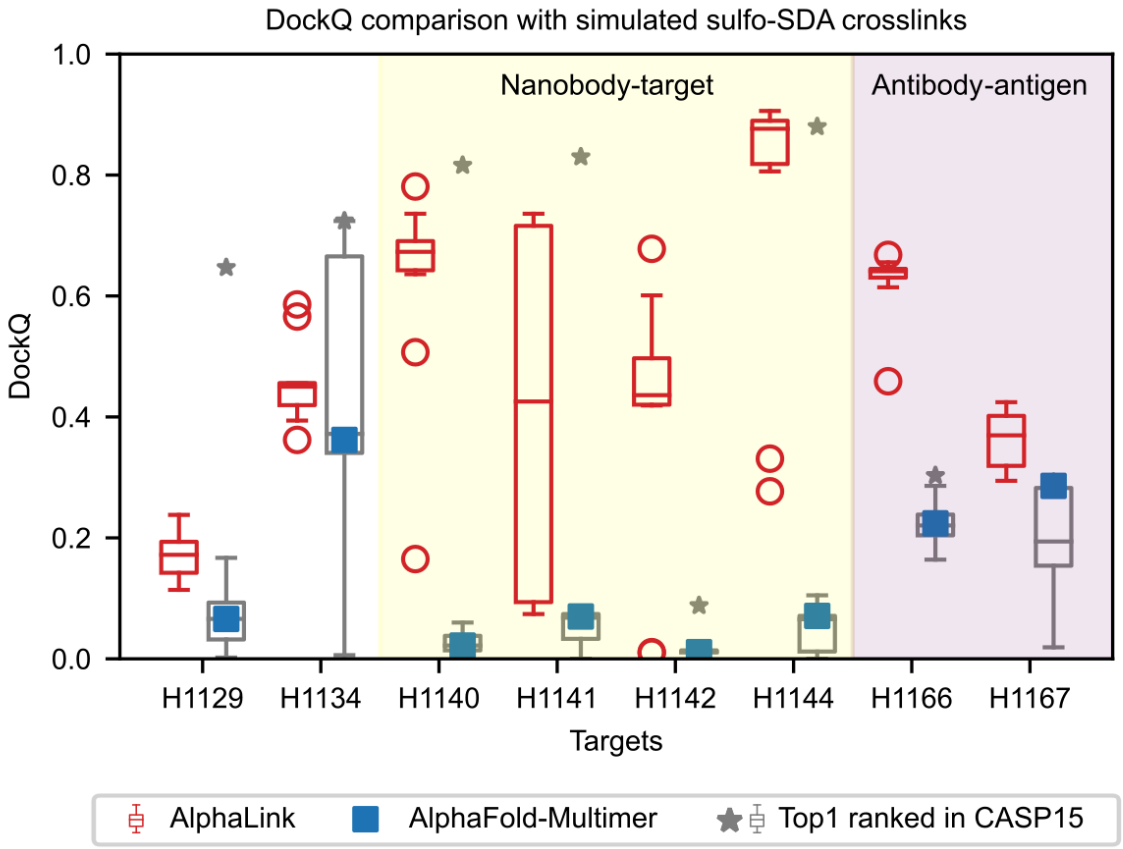

Extended Data Figure 1: DockQ comparison

DockQ comparison on 8 heteromeric CASP15 targets with simulated SDA crosslinks. The AlphaLink boxplot shows the highest model confidence model (N = 10) for 10 randomly sampled crosslink sets. The top ranked predictions (grey) correspond to all submissions that were ranked first by the participants (model_1), the best for each target is highlighted with an asterisk. AlphaFold-Multimer is highlighted in blue (model_1). The yellow shaded area highlights nanobody, the red shaded area antibody targets. In all boxplots, the line shows the median and the whiskers represent the 1.5x interquartile range.

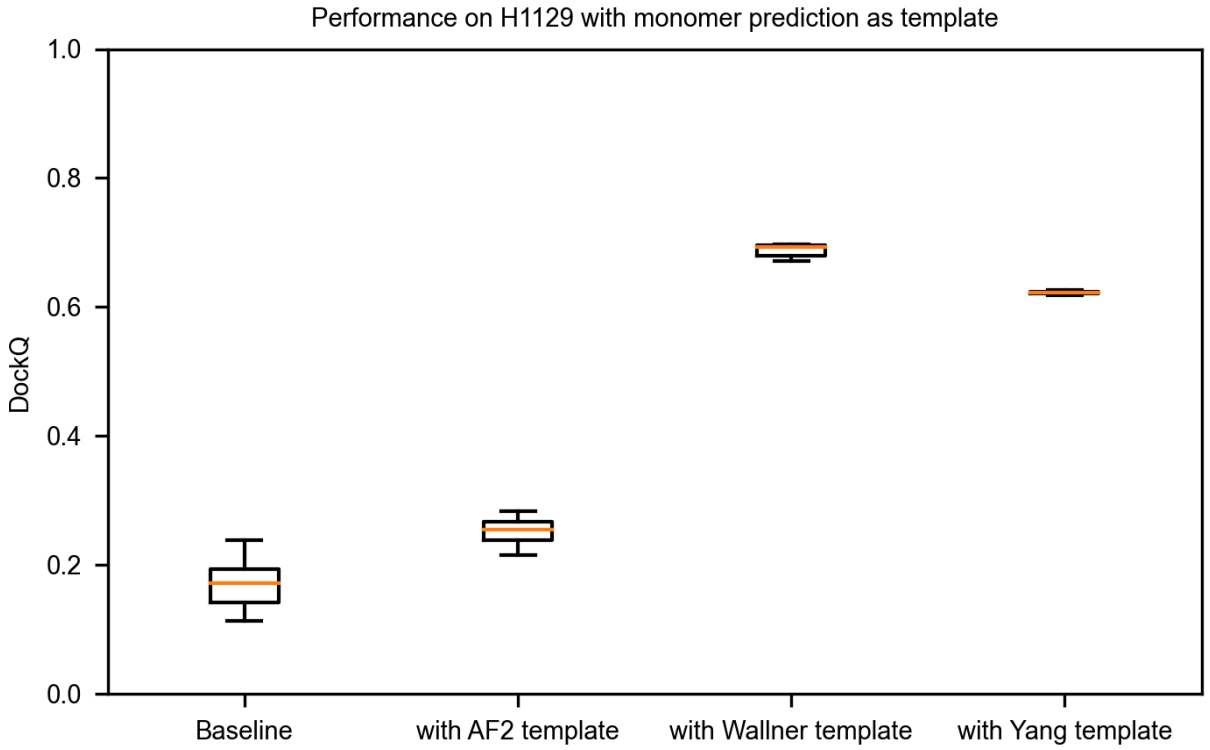

Extended Data Figure 2: Including monomer templates
Performance of AlphaLink with 10 samples and 3 recycling iterations on H1129. Baseline does fold-and-dock, the other runs include the top ranked monomer prediction of chain B from AF2, Wallner, or Yang as a template.

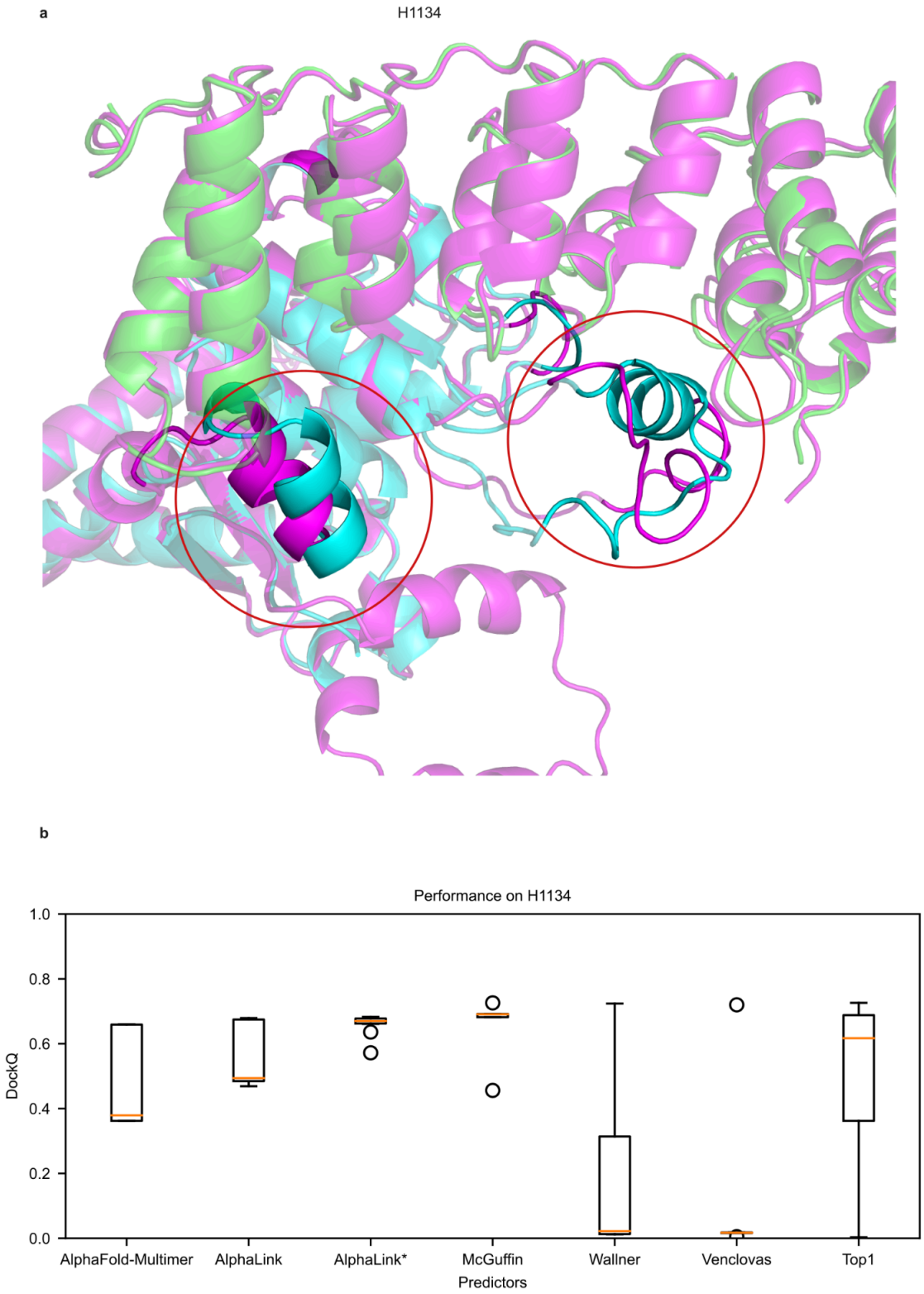

Extended Data Figure 3: Deviations in the interface for the H1134 AlphaLink prediction

a- Prediction of AlphaLink (purple) aligned to the native structure (cyan and green). There are few contacts in the interface, the alpha-helical region (red circle, right) is likely very flexible. The biggest deviations are highlighted by the red circle. **b-** DockQ scores of all submissions for the top predictors in CASP15 for H1134. Best in CASP15 corresponds to the best DockQ score per group. Most predictors show a large spread in prediction quality. In all boxplots, the line shows the median and the whiskers represent the 1.5x interquartile range. AlphaLink* selects the best prediction first by crosslink satisfaction and second by model confidence.

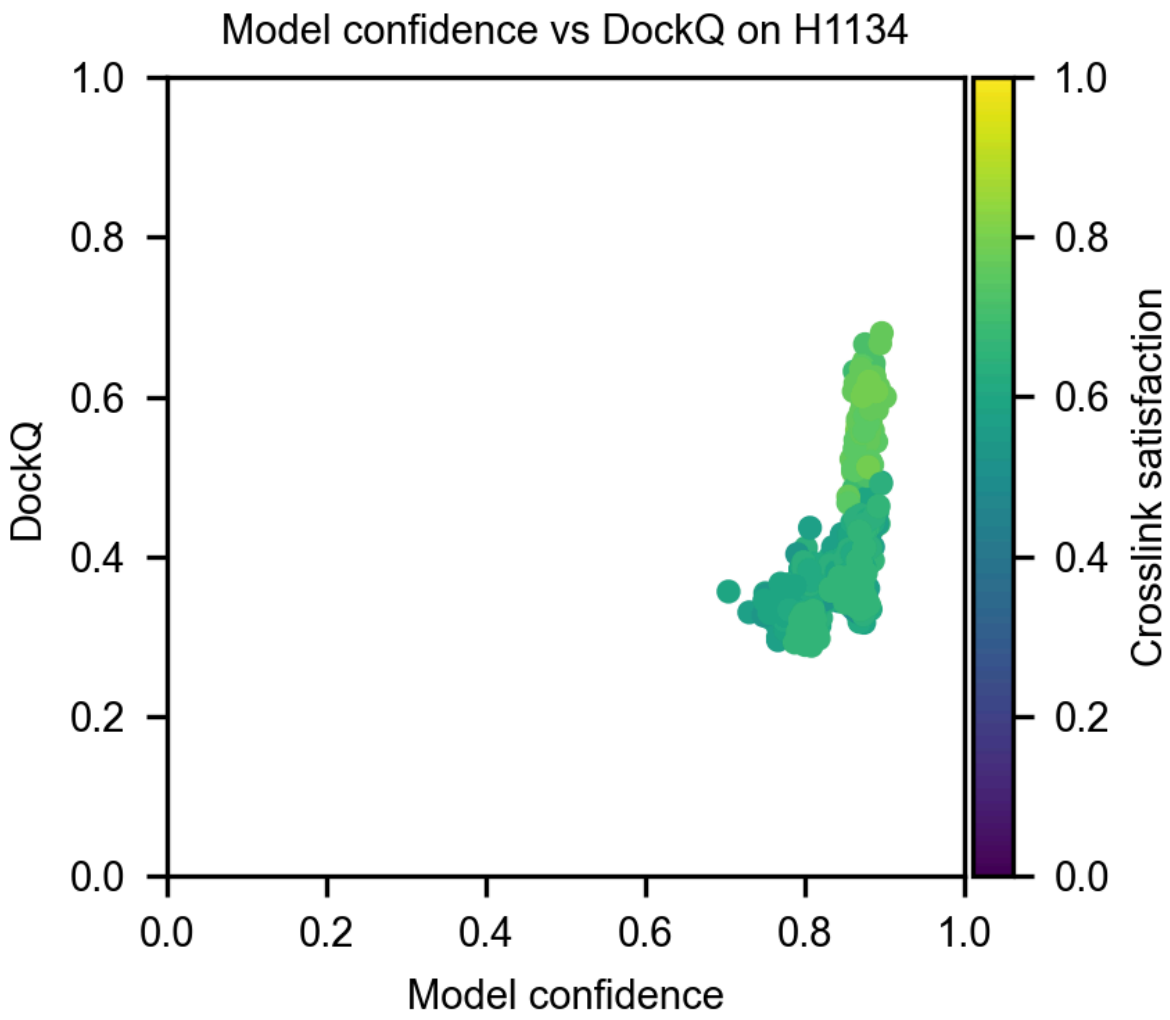

Extended Data Figure 4: AlphaLink model confidence - DockQ correlation on target H1134

Model confidence - DockQ correlation on H1134. We randomly subsampled N = 10 crosslink sets and generated M = 100 predictions per crosslink set with different seeds. One scatter point is one prediction. The colour gradient is showing the crosslink satisfaction.

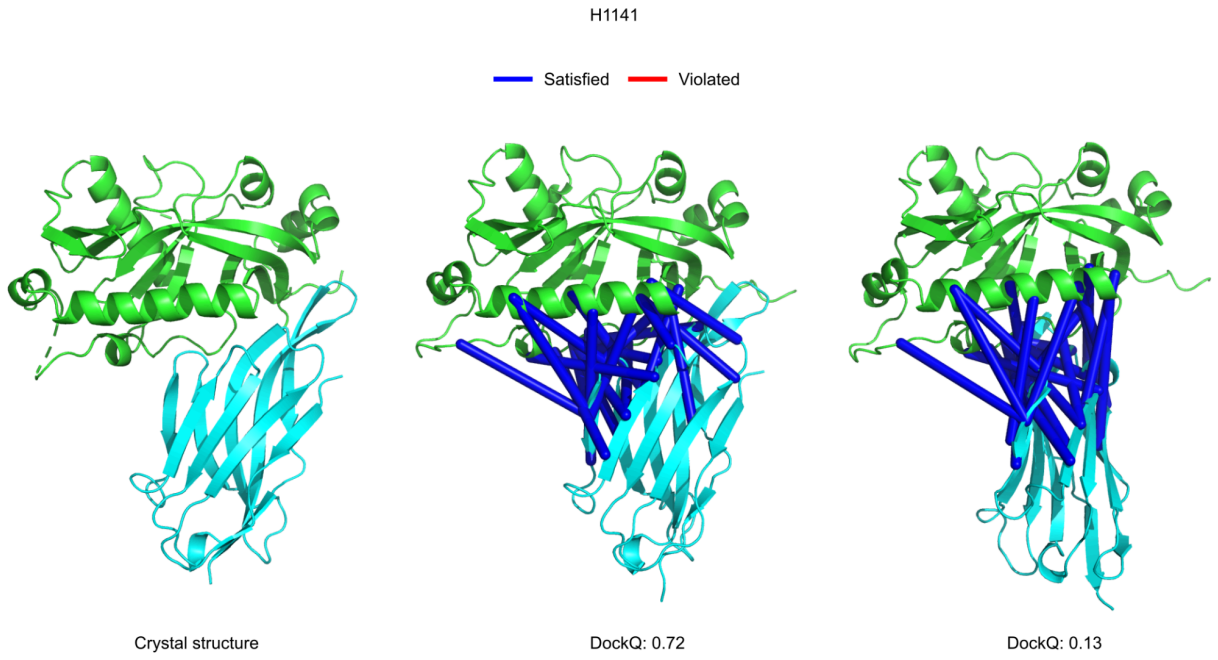

Extended Data Figure 5: Flexibility with SDA
Crystal structure (left) and AlphaLink predictions (middle and right) of H1141. We use the same crosslink set for both predictions. Crosslinks are completely satisfied (<25 Å) (blue). SDA's lower resolution allows predictions with vastly different DockQ scores.

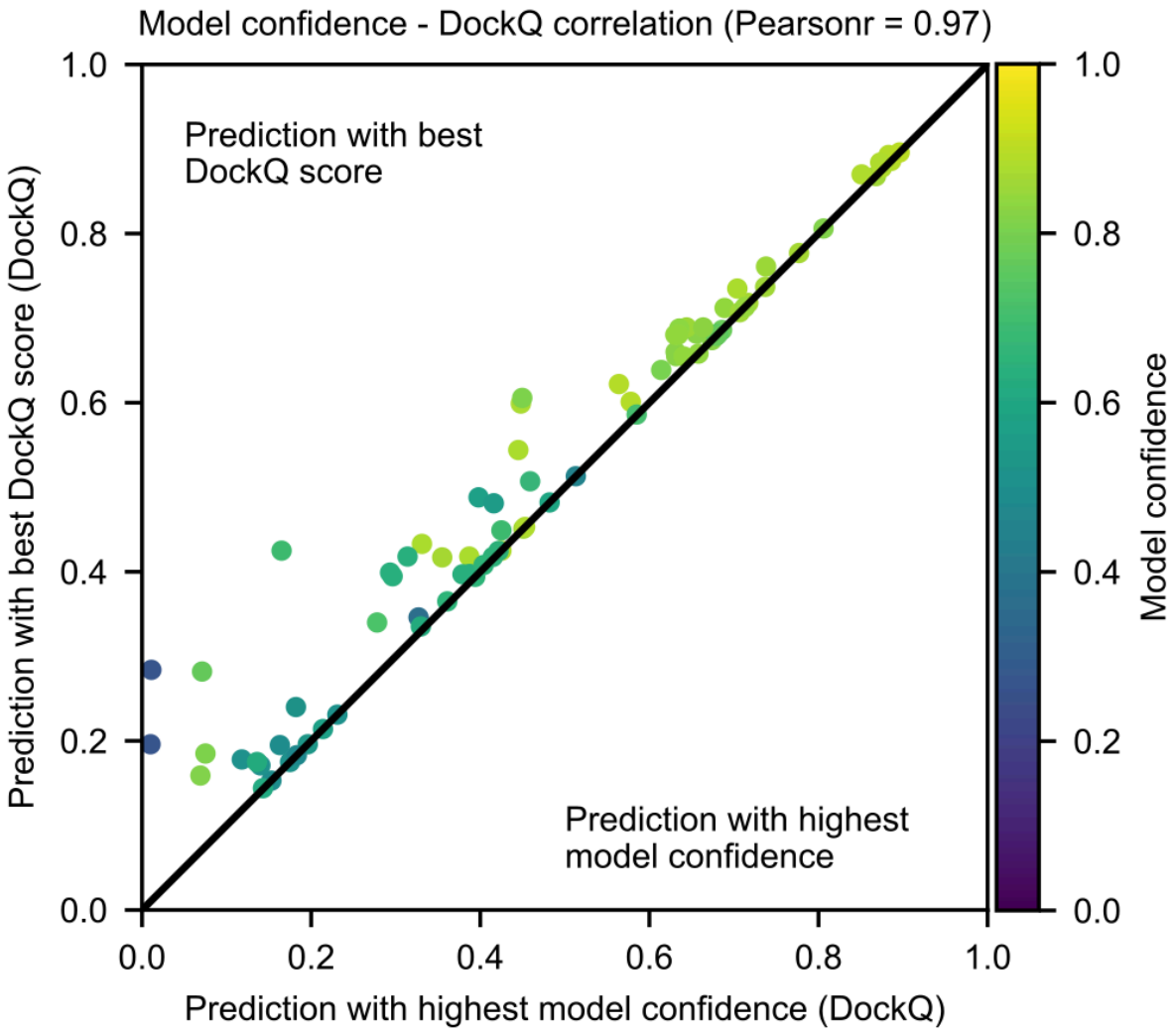

Extended Data Figure 6: Model confidence - DockQ correlation of AlphaLink on CASP15 targets

Model confidence - DockQ correlation on CASP15 targets (Pearsonr = 0.97). We randomly simulated 10 crosslink sets (33 links in the median) and generated 10 predictions per crosslink set with different seeds. One scatter point is one prediction. The colour gradient is showing the model confidence score.

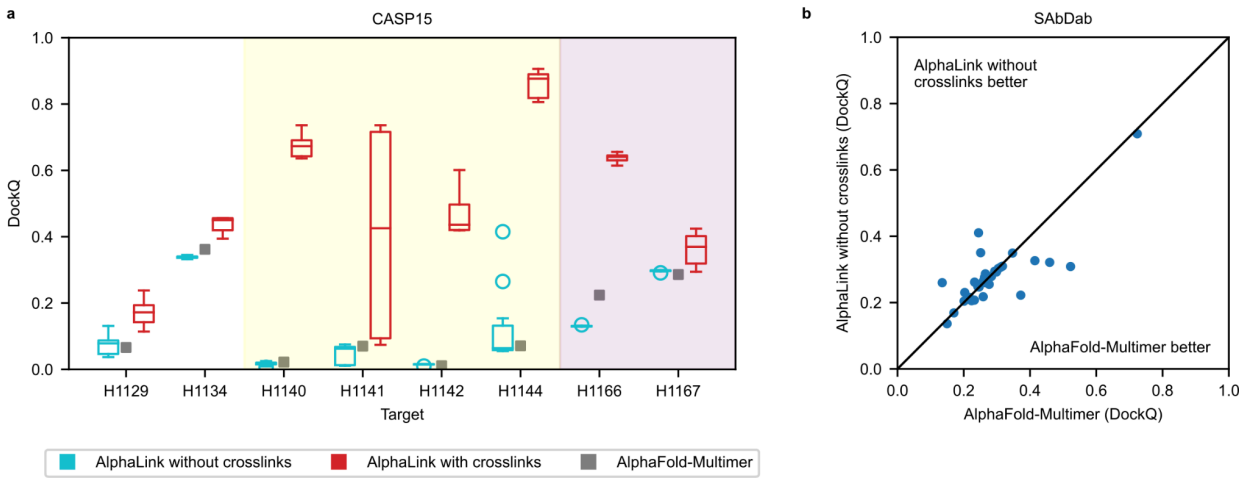

Extended Data Figure 7: AlphaLink performance with and without crosslinks
DockQ comparison on 8 heteromeric CASP15 targets with simulated SDA crosslinks. The AlphaLink boxplot shows the highest model confidence model (N = 10) for 10 randomly sampled crosslink sets. We predict the targets once with crosslinks (red) and once without crosslinks (cyan). The yellow shaded area highlights nanobody, the red shaded area antibody targets. In all boxplots, the line shows the median and the whiskers represent the 1.5x interquartile range.

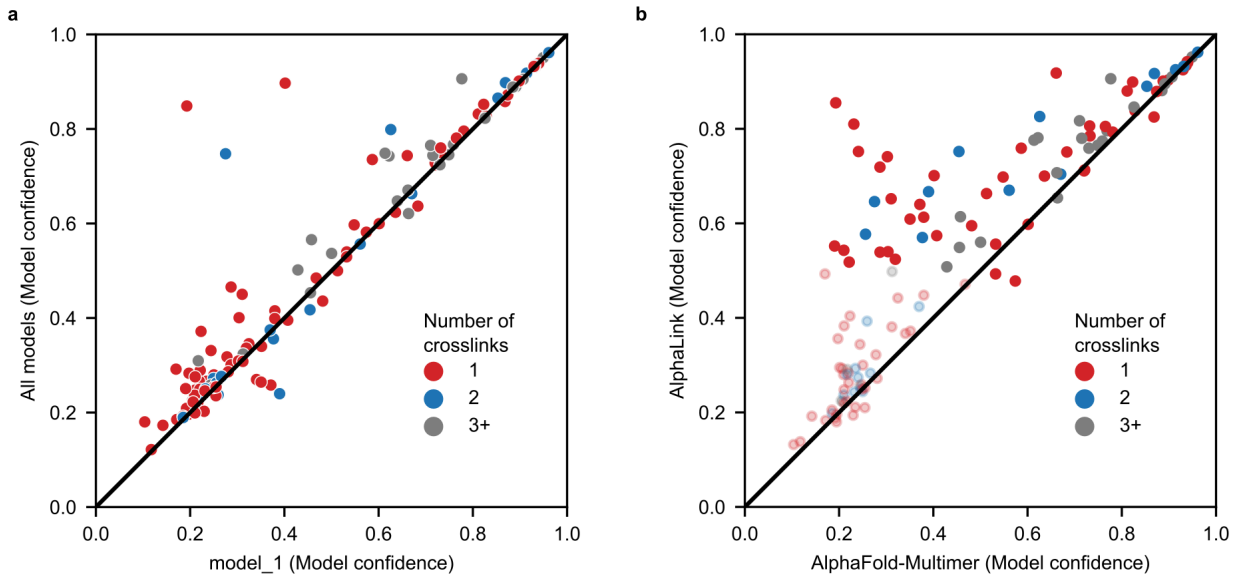

Extended Data Figure 8: Model_1 to all models

a- Highest model confidence of AlphaFold-Multimer v.2.2 on 134 protein-protein interactions from *Bacillus subtilis* with model_1…model_5 (N = 5) vs predicting the targets only with model_1 (M = 5). Using multiple models improves the model confidence in the mean by 0.03 points. **b-** Comparison of model_1 performance for AlphaFold-Multimer v2.2 and AlphaLink v2.2.

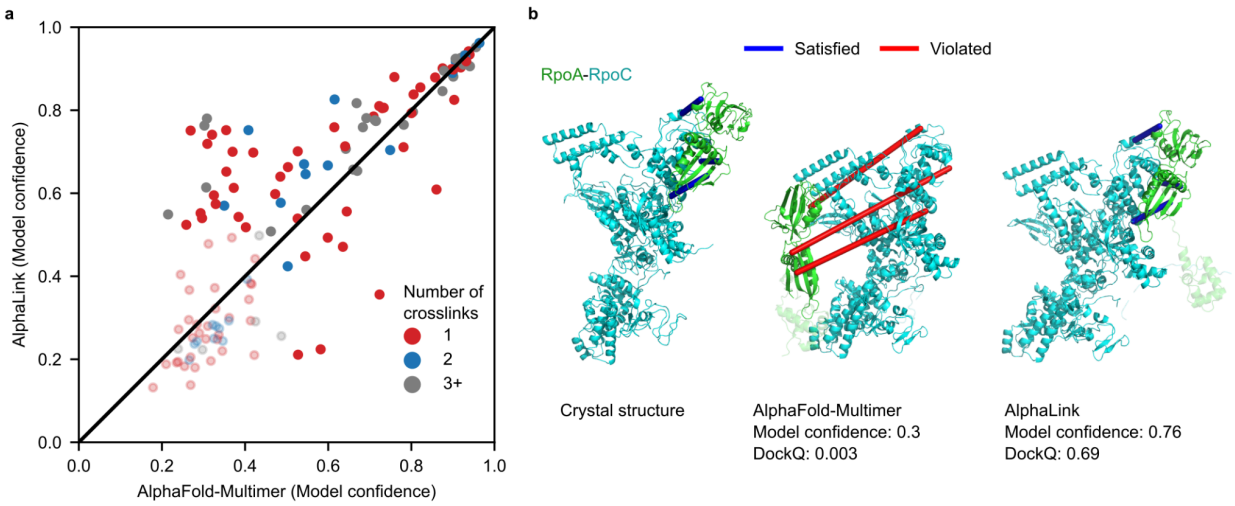

Extended Data Figure 9: Comparison with original data from *Bacillus subtilis* paper
a- Highest model confidence of AlphaLink trained on v2.2 weights (N = 5) vs AlphaFold-Multimer trained on v2.1 weights (M = 5) on the *Bacillus subtilis* data on K = 136 dimeric protein-protein interactions. Low confidence predictions for both methods (model confidence < 0.5) have higher transparency. Note that the model confidence might not be directly comparable between different network weights. **c-** Comparison of crystal structure (left), AlphaFold-Multimer prediction (middle) and AlphaLink prediction (right) for RpoA-RpoC with annotated crosslinks (blue - satisfied, red - violated).

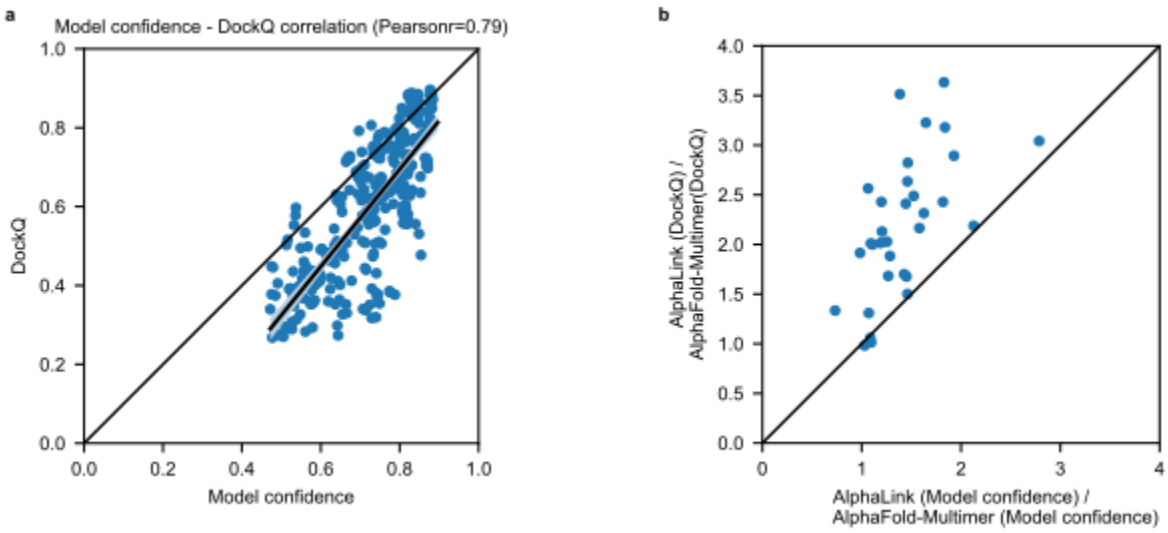

Extended Data Figure 10: Model confidence - DockQ correlation

a- Comparison of model confidence and DockQ for 33 antibody-antigen targets with 10 crosslink sets per target and five samples each. Best sample is picked by model confidence. The shaded area corresponds to the 95% confidence interval. Line shows the linear fit. **b-** Plotting the relationship of AlphaLink (DockQ) and AlphaFold-Multimer (DockQ) and the respective model confidences.